instruments

MDPI

Article

Fabrication of a Hydrogenated Amorphous Silicon Detector in 3-D Geometry and Preliminary Test on Planar Prototypes

Mauro Menichelli [1,*], Marco Bizzarri [1,2], Maurizio Boscardin [3,4], Mirco Caprai [1], Anna Paola Caricato [5], Giuseppe Antonio Pablo Cirrone [6], Michele Crivellari [4], Ilaria Cupparo [7], Giacomo Cuttone [6], Silvain Dunand [8], Livio Fanò [1,2], Omar Hammad Alì [4], Maria Ionica [1], Keida Kanxheri [1], Matthew Large [9], Giuseppe Maruccio [5], Anna Grazia Monteduro [5], Francesco Moscatelli [1,10], Arianna Morozzi [1], Andrea Papi [1], Daniele Passeri [1,11], Marco Petasecca [9], Silvia Rizzato [5], Alessandro Rossi [1,2], Andrea Scorzoni [1,11], Leonello Servoli [1], Cinzia Talamonti [7], Giovanni Verzellesi [3,12] and Nicolas Wyrsch [8]

1 INFN, Sez. di Perugia, via Pascoli s.n.c., 06123 Perugia, Italy; marco.bizzarri@unipg.it (M.B.); mirco.caprai@pg.infn.it (M.C.); livio.fano@pg.infn.it (L.F.); maria.ionica@pg.infn.it (M.I.); keida.kanxheri@pg.infn.it (K.K.); francesco.moscatelli@pg.infn.it (F.M.); arianna.morozzi@pg.infn.it (A.M.); andrea.papi@pg.infn.it (A.P.); daniele.passeri@unipg.it (D.P.); alessandro.rossi@pg.infn.it (A.R.); andrea.scorzoni@unipg.it (A.S.); leonello.servoli@pg.infn.it (L.S.)
2 Dipartimento di Fisica e Geologia dell'Università degli Studi di Perugia, via Pascoli s.n.c., 06123 Perugia, Italy
3 INFN, TIPFA Via Sommarive 14, 38123 Povo, TN, Italy; boscardi@fbk.eu (M.B.); giovanni.verzellesi@unimo.it (G.V.)
4 Fondazione Bruno Kessler, Via Sommarive 18, 38123 Povo, TN, Italy; crivella@fbk.eu (M.C.); ohammadali@fbk.eu (O.H.A.)
5 INFN and Department of Mathematics and Physics "Ennio de Giorgi" University of Salento, Via per Arnesano, 73100 Lecce, Italy; Annapaola.Caricato@le.infn.it (A.P.C.); giuseppe.maruccio@unisalento.it (G.M.); annagrazia.monteduro@unisalento.it (A.G.M.); silvia.rizzato@unisalento.it (S.R.)
6 INFN Laboratori Nazionali del Sud, Via S.Sofia 62, 95123 Catania, Italy; pablo.cirrone@infn.it (G.A.P.C.); giacomo.cuttone@lns.infn.it (G.C.)
7 INFN and Dipartimento di Fisica Scienze Biomediche sperimentali e Cliniche "Mario Serio", Viale Morgagni 50, 50135 Firenze, FI, Italy; ilaria.cupparo@unifi.it (I.C.); cinzia.talamonti@unifi.it (C.T.)
8 Ecole Polytechnique Fédérale de Lausanne (EPFL), Institute of Microengineering (IMT), Rue de la Maladière 71b, 2000 Neuchâtel, Switzerland; sylvain.dunand@epfl.ch (S.D.); nicolas.wyrsch@epfl.ch (N.W.)
9 Centre for Medical Radiation Physics, University of Wollongong, Northfields Ave, Wollongong, NSW 2522, Australia; mjl970@uowmail.edu.au (M.L.); marcop@uow.edu.au (M.P.)
10 CNR-IOM, via Pascoli s.n.c., 06123 Perugia, Italy
11 Dipartimento di Ingegneria dell'Università degli studi di Perugia, via G.Duranti, 06125 Perugia, Italy
12 Dipartimento di Scienze e Metodi dell'Ingegneria, Università di Modena e Reggio Emilia, Via Amendola 2, 42122 Reggio Emilia, Italy
* Correspondence: mauro.menichelli@pg.infn.it

Abstract: Hydrogenated amorphous silicon (a-Si:H) can be produced by plasma-enhanced chemical vapor deposition (PECVD) of SiH_4 (silane) mixed with hydrogen. The resulting material shows outstanding radiation hardness properties and can be deposited on a wide variety of substrates. Devices employing a-Si:H technologies have been used to detect many different kinds of radiation, namely, minimum ionizing particles (MIPs), X-rays, neutrons, and ions, as well as low-energy protons and alphas. However, the detection of MIPs using planar a-Si:H diodes has proven difficult due to their unsatisfactory S/N ratio arising from a combination of high leakage current, high capacitance, and limited charge collection efficiency (50% at best for a 30 μm planar diode). To overcome these limitations, the 3D-SiAm collaboration proposes employing a 3D detector geometry. The use of vertical electrodes allows for a small collection distance to be maintained while preserving a large detector thickness for charge generation. The depletion voltage in this configuration can be kept below 400 V with a consequent reduction in the leakage current. In this paper, following a detailed description of the fabrication process, the results of the tests performed on the planar p-i-n structures made with ion implantation of the dopants and with carrier selective contacts are illustrated.

Citation: Menichelli, M.; Bizzarri, M.; Boscardin, M.; Caprai, M.; Caricato, A.P.; Cirrone, G.A.P.; Crivellari, M.; Cupparo, I.; Cuttone, G.; Dunand, S.; et al. Fabrication of a Hydrogenated Amorphous Silicon Detector in 3-D Geometry and Preliminary Test on Planar Prototypes. *Instruments* **2021**, *5*, 32. https://doi.org/10.3390/instruments5040032

Academic Editor: Antonio Ereditato

Received: 23 July 2021
Accepted: 28 September 2021
Published: 8 October 2021

Keywords: solid-state detectors; position detectors; radiation hard detector; hydrogenated amorphous silicon; 3D detector

1. Introduction

Hydrogenated amorphous silicon (a-Si:H) is a disordered semiconductor obtained via plasma-enhanced chemical vapor deposition (PECVD) of a mixture of silane (SiH_4) and hydrogen at temperatures of 250–300 °C [1]. The resulting material has an irregular arrangement of atoms resulting in not all Si–Si bonds being saturated, leading to the presence of dangling bonds (DBs) that are related to the presence of intermediate states between the valence and the conduction bands. The introduction of hydrogen into the mixture has the purpose of passivating most of these dangling bonds. In amorphous (non-hydrogenated) silicon (a-Si), the density of defects due to DBs is 10^{19} cm^{-3}, whereas for a-Si:H this density can be as low as 10^{15} cm^{-3}. Although the amount of hydrogen necessary to reach these levels of DB passivation is approximately 1% atomic, device-grade a-Si:H usually exhibits hydrogen concentrations between 4% and 12%. The hydrogen percentage in the material affects its bandgap (increasing the hydrogen percentage leads to a larger bandgap) and depends on deposition conditions such as processing temperature. However, temperatures above 350 °C lead to hydrogen desorption, transforming the material into a-Si. This relatively low deposition temperature facilitates the adhesion of a-Si:H on many different substrates, like glass (including Pyrex and fused silica), stainless steel, crystalline silicon, silicon oxide, aluminum, coated ceramic, chromium-plated brass, copper-coated printed circuit board (PCB), and organic materials like polyammide, PEN (polyethylene naphthalate), PET (polyethylene terephthalate) and PI (polymide), heat-resistant organics/inorganic polymers (like ormocer®), and even on top of electronic devices in CMOS (complementary metal-oxide semiconductor) technology [2]. Usual deposition techniques for detector-quality a-Si:H are PECVD with plasma excitation at radio frequency (13.56 MHz) [3], very high frequencies (between 27 and 150 MHz) [4] or even with microwave frequencies [5], and hot-wire deposition [6].

The relatively wide bandgap of a-Si:H and its disordered nature results in a low charge carrier mobility (1–3 cm^2 V^{-1} s^{-2} for electrons and 0.01 cm^2 V^{-1} s^{-2} for holes) and a charge collection time in a 30 µm-thick diode of below 15 ns [7]. A-Si:H is a semi-isolating material with a resistivity of above 10^{10} Ω cm. This resistivity can be lowered by more than seven orders of magnitude by doping [8]. However, doping of a-Si:H creates additional defects, which consequently lowers the carrier lifetime of the material [9]. Therefore, doped layers cannot be used as active layers in photodiodes or particle sensors. For this reason, p-i-n diode structures, not direct p–n junctions, are preferred with relatively thin p- or n-doped layers. Usually, this material is doped with the addition of PH_3 (n-type doping) or B_2H_6 or trimethylboron (p-type doping) in the process gas mixture. It was also demonstrated that similar doping levels and conductivity can be achieved by ion implantation at low temperatures [10]. This doping technique was demonstrated by the fabrication of various devices [11,12]. The feature of a-Si:H that makes it attractive for particle detector developments is its remarkable radiation hardness. This has led to significant research activities aiming at single minimum ionizing particle (MIP) detection [13–15]. In Ref. [16] the radiation tests of a 32.6 µm-thick p-i-n diode irradiated at CERN's Proton-Synchrotron with 24 GeV protons up to a maximum fluence of 7×10^{15} p/cm^2 is reported; an increment in leakage current of a factor of 2 at 9×10^4 V/cm electric field was observed, and this increase disappeared after 24 h of annealing at 100 °C. Although this material has an extremely high radiation hardness, the main limitation of a-Si:H planar detectors is their poor signal-to-noise ratio for the detection of MIPs, which is yet to exceed a value of 5. The reason for this low S/N ratio is the very high depletion voltage (with electric fields up to 10^5 V/cm) that generates a high leakage current (up to about 1 $\mu A/cm^2$). Furthermore, the low charge collection efficiency (below 50% for a 30 µm-thick diode) due to the disordered

nature of the a-Si:H lattice structure contributes to the decrease in the overall value of the signal-to-noise ratio even if some effort has been performed to increase the charge collection efficiency in these devices [17]. The depletion voltage of an a-Si:H detector V_d is related to the density of DBs (N_{db} number of dangling bonds/volume in cm^3) according to the following formula:

$$V_d = \frac{e \times N_{db} \times d^2}{2\varepsilon}$$

where e is the electron charge and d is the thickness of the depleted layer. If we express d in µm and V_d in volts this formula becomes $V_d = k \times d^2$, where k ranges from 0.3 to 1.2 when N_{db} ranges from 5×10^{14} to 2×10^{15} cm^{-3}. Furthermore, a large thickness of the detector reduces the charge collection efficiency due to charge trapping over a longer distance.

Increasing the depletion voltage increases the leakage current at full depletion, and this increases the noise. To reduce noise and increase the signal we propose fabricating a p-i-n-structured a-Si:H detector in 3D geometry that makes it possible to keep a relatively small collection distance (namely, a 25–35 µm inter-electrode spacing) with a detector thickness of up to 100 µm or more, increasing the total charge generated in the detector by an MIP. Maintaining a small distance between the electrodes is important for keeping the leakage current low, hence reducing the noise. In Figure 1 we show the baseline design for our detector, where a-Si:H is deposited over a low-resistivity p-type silicon substrate that distributes the bias to the p-type electrodes on the detector. The n-type electrode collects the signal for the readout electronics connected on the top contacts. This configuration is the basis of development for Si-3D for high-luminosity (HL) LHC applications. [18]. Figure 2a depicts the electrode arrangement as seen from a top-down perspective, where one n-type finger-type electrode is surrounded by four p-type finger-type electrodes. Additionally, Figure 2 shows alternative electrode configurations: Figure 2a is the baseline configuration, Figure 2b shows a configuration with eight p-type finger-type electrodes surrounding an n-type electrode, Figure 2c shows a configuration with one finger-type n-type electrode surrounded by four trench-type p-type electrodes, and Figure 2d shows all alternate trench n-type and p-type electrodes. Trench electrode configurations have been studied and used for the realization of excellent time-resolution silicon detectors, for example in the TIMESPOT collaboration. [19]. Table 1 shows a comparison between a-Si:H and c-Si physical parameters.

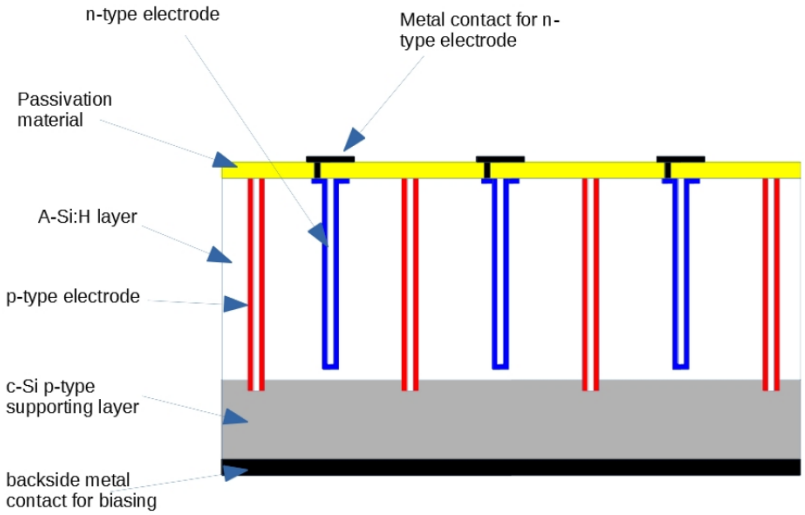

Figure 1. Baseline configuration of an a-Si:H detector. P-type electrodes are biased from the p-doped c-Si substrate, whereas n-type electrodes are connected to the readout electronics.

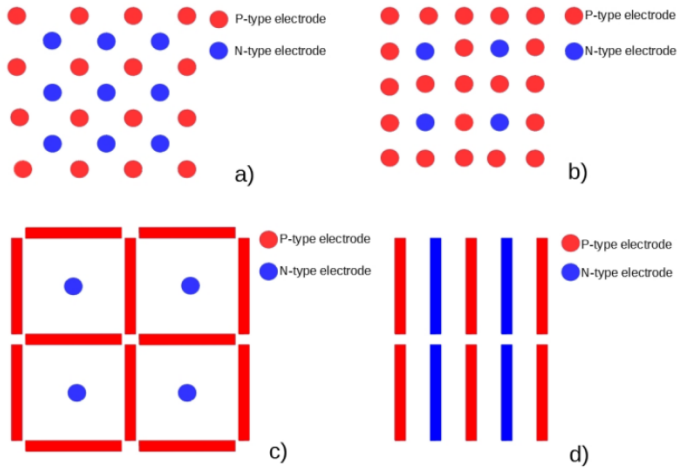

Figure 2. 3D a-Si:H detector configurations: (**a**) finger-type n-doped electrode surrounded by 4 finger-type p-doped electrodes, (**b**) finger-type n-doped electrode surrounded by 8 finger-type p-doped electrodes, (**c**) finger-type n-doped electrode surrounded by 4 trench-type p-doped electrodes, (**d**) all trench configurations.

Table 1. Summary of c-Si and a-Si:H characteristics.

Properties	c-Si	a-Si:H	Remarks
Bandgap (eV)	1.14	1.65–1.8 (for device grade)	For a-Si:H given by Tauc's gap, depends on H content
Density (g/cm^3)	2.3290	2.20–2.31 (device grade)	
Hydrogen content (at. %)	0	4–15% (device grade)—up to 50% possible	
e-h creation energy (eV)	3.6	4–6	
e-h creation/μm for MIP	~80 (1)	~80	Stopping power similar (almost same density, effect of H negligible)
e drift mobility ($cm^2s^{-1}V^{-1}$)	1450	1–3	
h drift mobility ($cm^2s^{-1}V^{-1}$)	450	0.01	
e mobility lifetime (cm^2V^{-1})	~5×10^{-3}	$\leq 5 \times 10^{-5}$	For a-Si:H, depends on deposition and treatments
h mobility lifetime (cm^2V^{-1})	~3×10^{-3}	$\leq 10^{-7}$	For a-Si:H, depends on deposition and treatments
Full depletion field (V/μm)	<1	≥10	Depends on defect density
Charge collection efficiency	97–99%	40–50% (2)	Depends on charge type, field, and time window
Device leakage current not irradiated (A/cm^3)	10^{-3}–10^{-5}	$\leq 10^{-3}$ (3)	For a-Si:H, thickness and field dependent (a-Si:H bulk, for 10 μm-thick diode at field of 10^5 V/cm, non-irradiated)
Device leakage current irradiated 5×10^{15} p (24 GeV)/cm^2) (A/cm^3)	10^{-1}–10^{-3}	<3 10^{-3} (4)	For a-Si:H, thickness and field dependent (a-Si:H bulk, for 10 μm-thick diode at field of 10^5 V/cm,

(1) Experimentally observed value. Theoretical value is 108 for a stopping value of 1.66 MeV cm^2 g^{-1} for an MIP in c-Si. (2) For transient experiment. Due to deep trapping, holes are, in principle, not collected. Collection efficiency >80% in steady state. (3) Leakage value for planar diode. Diode on non-planar substrates and unpassivated edges can lead to significantly higher leakage. (4) Experimental value not available. Increase of leakage by 2–3 for 32 μm-thick diodes.

2. The Fabrication of a 3D Detector

The fabrication of a 3D detector in a-Si:H is somewhat different than the construction of a 3D detector in crystalline silicon due to the constraint of keeping the temperature of processing below 250–300 °C in order to avoid hydrogen desorption.

The process starts with the deposition on support wafers (typically a Cz p-type silicon wafer with a resistivity below 10 Ωcm) of the a-Si:H performed via PECVD with a VHF-excited plasma at the frequency of 70 MHz. The plasma is composed of a mixture of silane and hydrogen (ratio of 1 to 1) at temperatures around 200 °C and will produce a layer with a thickness of around 100 µm.

After that, both the ohmic and junction columns are defined and etched using a deep reactive ion etching (DRIE) apparatus based on the Bosh process. This technique allows for the etching of a hole with a diameter of a few microns and with a high aspect ratio (more than 50). The ohmic columns are etched deeper than the a-Si:H layer (partially etching the c-Si substrate) and the junction columns are etched to approximately 20 µm shallower than the a-Si:H thickness.

Afterwards, the etched holes in the a-Si:H layer must be doped in the internal surfaces. In order to create the p-i-n structure in the detector, two independent masks are fabricated to define an n-plus region and a p-plus region. Doping the detector inside the holes cannot be performed using common techniques for planar structures (i.e., PECVD deposition of doped a-Si:H) as these deposition techniques cannot achieve the required conformality in deep trenches [20,21]. Therefore, two doping options are considered:

- **Option 1:** atomic layer deposition (ALD) of conductive metallic oxides for the creation of selective contacts for each type of charge carriers: titanium oxide for electron-selective contacts and tungsten or molybdenum oxide for hole-selective contacts. Since the oxides for charge-selective contacts are quite resistive, depositing a conductive metal inside the holes or trenches by PLD (pulsed laser deposition) is foreseen.
- **Option 2:** ion implantation of boron (p-type doping) and phosphorous (n-type doping) followed by a temperature activation annealing process below 200 °C or an additional metal deposition by PLD if needed.

In order to have a reasonable time constant (order of 10 ns) for charge collection, the resistance of the electrodes should be in the order 1 MΩ.

After the doping, a contact hole is opened and the metal (typical Al 1% silicon) is deposited and defined. The passivation, based on a multilayer of Si_3N_4 and SiO_2, is deposited by the low-temperature PECVD technique and subsequently opened to allow the contact of the metal layer. The final step is the metal deposition of the backside that is used as bulk bias contact.

3. Results of the Phase I Prototype

The complexity of the proposed 3D detector geometries presents many technological challenges regarding fabrication. The construction of prototype devices allows for the challenges of 3D a-Si:H device fabrication to be addressed in a sequential manner. Phase 1 prototypes feature a planar p-i-n architecture and aim to assess the feasibility of the doping options introduced in the previous chapter. Measurements investigate the performance of the doped device layers to produce an efficient junction for biasing the intrinsic layer and provide an effective charge collection and current rectification. A second generation of prototypes (under design) aims to accurately measure the relation between the hole diameter and the rate at which a-Si:H is etched via DRIE. The proposed 3D geometries require the p-type electrodes to be embedded at a sufficient depth to erase a shallow layer of the a-Si:H substrate, and the n-type electrodes are to be fully contained within the a-Si:H device layer (Figure 3). Therefore, second-generation prototypes aim to assess the feasibility of etching p-type and n-type electrodes in a single process, exploiting the feature of the DRIE process in which larger-diameter holes turn out to have a faster etching rate.

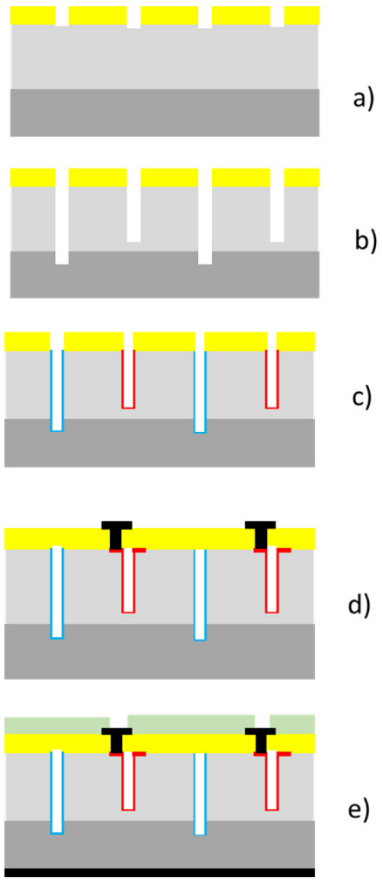

Figure 3. Process description of 3D a-Si:H detector fabrication (option 2); lithographic steps are omitted. (**a**) Silicon nitride passivation layer deposition and patterning for the DRIE process. (**b**) P-hole and n-hole etching. (**c**) Columns doping by ion implantations. (**d**) Opening of contacts, metal deposition, and etching. (**e**) Deposition and patterning of passivation layer and deposition of backside metal.

All measurements in this section were taken using a Keithley 237 Source-Measure Unit (SMU).

3.1. Leakage Current Test on Option 1

Concerning option 1, related to the use of selective contacts, vertical structures were fabricated on chromium-plated glass substrates. As electron-selective contacts, ZnO:Al (aluminum-doped zinc oxide (AZO)) and TiO_2 (respectively, 60 nm and 10 nm thick) layers were implemented on the substrate side and compared. As a hole-selective contact, MoO_x (20 nm thick) protected by an indium thin oxide layer (60 nm) was deposited. All selective contacts were deposited by sputtering. Note that for 3D architecture, ALD should be used to enable conformal deposition in the holes or trenches.

Figure 4 depicts the initial I/V measurements performed on two vertical diodes with a sensitive area of 0.25 cm^2, providing comparisons between the two different materials employed as electron-selective contacts. The results of both vertical diode structures displayed exceptional rectifying behaviors. The generated leakage currents in TiO_2 and AZO electron-selective contact devices at −5 V applied bias were measured as two and three orders of magnitude larger than the leakage currents under +5 V bias, respectively. Furthermore, the obtained leakage current of approximately 4 nA/cm^2 in both devices at +40 V bias is comparable to that obtained in samples fabricated via ion-implantation doping. Thus, this doping technique is identified as an acceptable alternative to implantation and will be explored in detail in future studies.

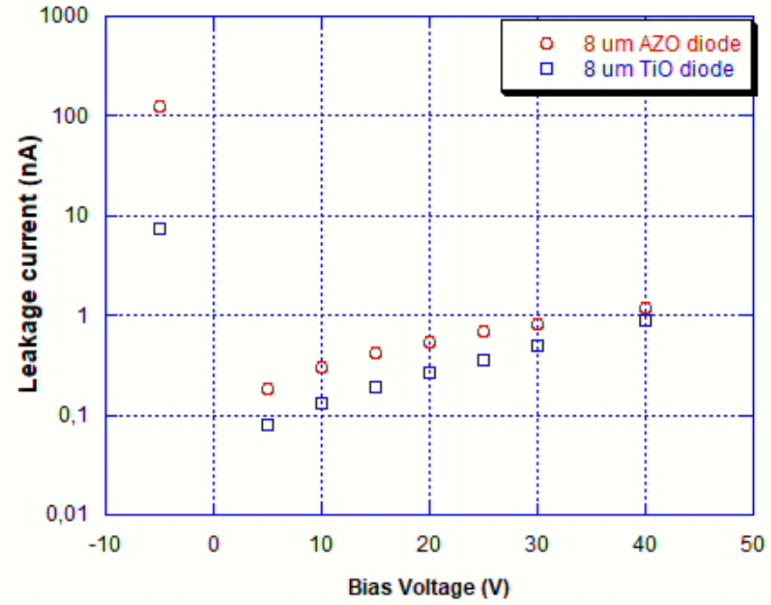

Figure 4. Leakage current vs. bias field for 2 vertical detectors with charge-selective contacts of 8 μm thickness biased up to 5 V/μm electric field: One of the samples was fabricated using TiO_2 electron-selective contact and the other sample was fabricated using ZnO:Al (AZO) electron-selective contact. MoO_x/ITO are used in both devices as hole−selective contacts.

3.2. Leakage Current Tests on Doping Option 2

In order to verify the feasibility of performing a doping process inside the holes fabricated via the DRIE process to form effective 3D p- and n-type electrodes, the two doping options explained in the previous section were verified with the construction of two types of prototypes: vertical diodes and lateral diodes in a planar configuration, obtained from the deposition of a layer of 10 μm of a-Si:H on a heavily doped p-type c-Si substrate (300 μm thickness).

Vertical diodes, shown in Figure 5, used the p-type c-Si silicon substrate as the p-type biasing electrode and the n-type electrode was obtained via ion implantation of phosphor ions. Diodes with several geometries were produced, namely, single diodes, 2 × 3 diode arrays, 2 × 10 diode arrays, and strip detectors.

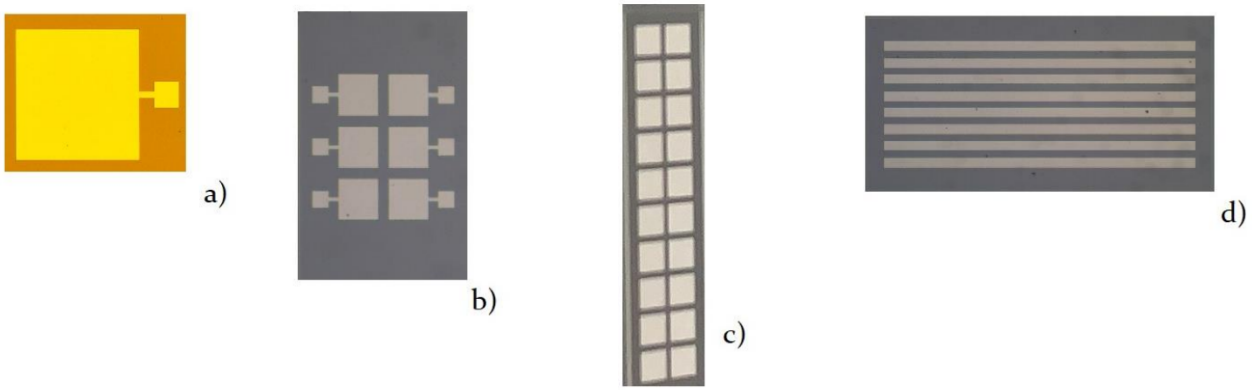

Figure 5. Vertical diode configurations: (**a**) single diode of 1.25 × 1.25 mm^2, (**b**) 2 × 3 diode array, (**c**) 2 × 10 diode array, and (**d**) 8-strip device.

Figure 6 shows an I/V test on two samples of a 4 mm^2 vertical diode. As shown in the figure, the diode acted as a rectifying junction and the leakage current with 50V bias was about 147 pA with a current density of 3.6 nA/cm^2 on the best sample.

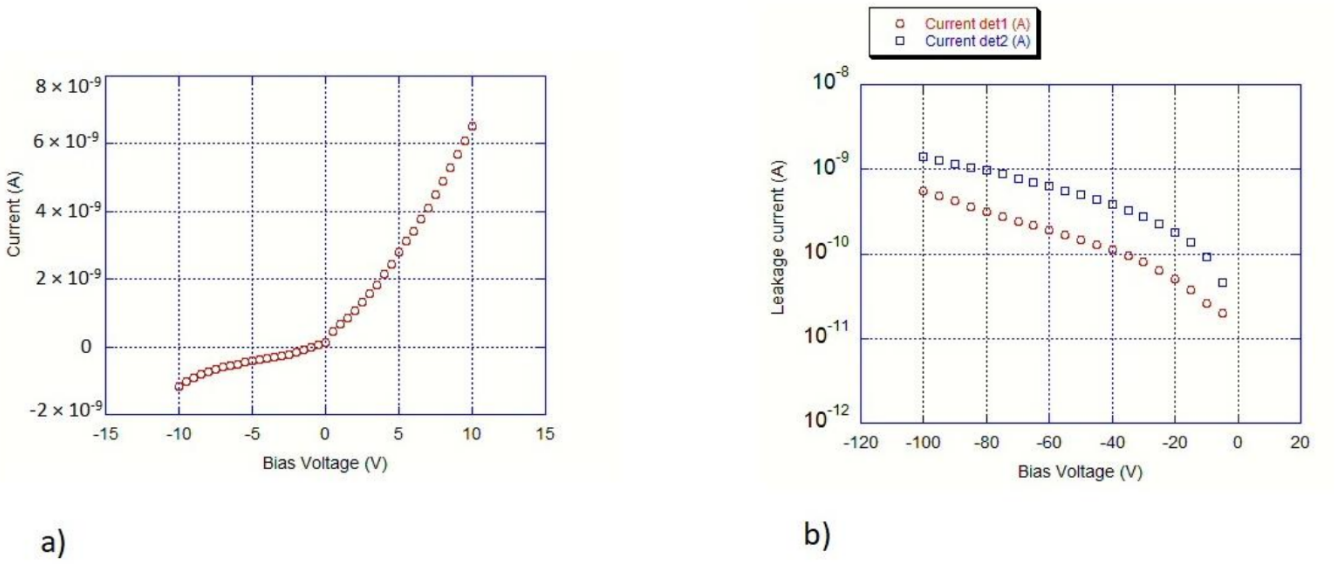

Figure 6. (**a**) I/V plot on a vertical 4 mm^2 diode where the rectifying behavior is apparent. (**b**) Reverse current versus bias voltage on two detector samples at 50 V leakage currents are 147 and 496 pA for det 1 and det 2, respectively, corresponding to current densities of 3.6 and 12.4 nA/cm^2.

Figure 7 presents the various configurations and geometries of the lateral diode structures. These lateral diodes were fabricated with the p-type and n-type electrodes deposited on the surface of the a-Si:H layer and a thin (500 nm) layer of silicon oxide separating this a-Si:H layer from the silicon substrate. The sensitive region of the lateral diodes existed between the p- and n-type electrodes, which were doped with boron and phosphorous, respectively.

Figure 7. Lateral diode configurations: (**a**) strip detector, (**b**) comb and strip detectors (the comb is p-doped whereas the strips are n-doped), (**c**) double comb detector, (**d**) circular device (the central electrode is n-type whereas the external electrode is p-type, (**e**) 3 × 3 array of circular detectors.

In comparison to the I/V characteristics of the vertical diodes (Figure 6), the I/V curves of the lateral diodes in Figure 8 displayed an even more pronounced rectifying behavior and exceptionally low leakage current values, ranging from 339 pA (best small detector) to 1030 pA (worst large detector).

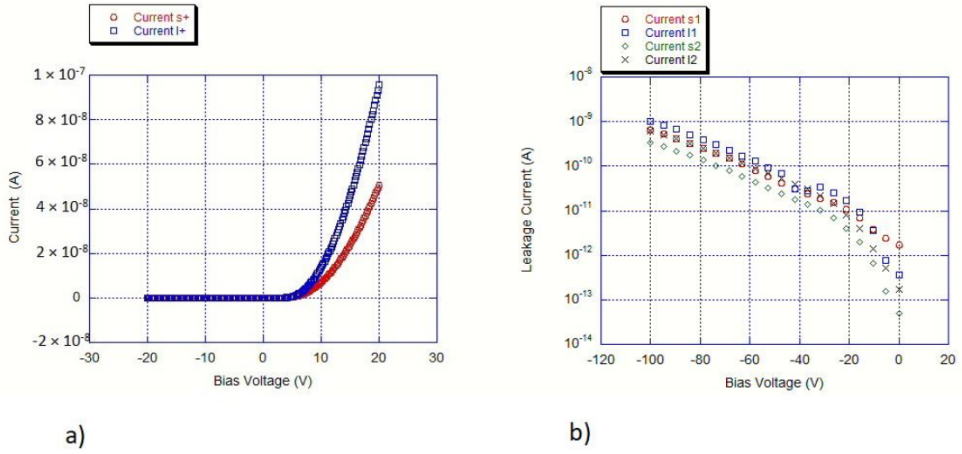

Figure 8. Leakage current vs. bias voltage in lateral detectors: (**a**) direct and reverse biasing, (**b**) reverse bias only.

4. Testing with X-ray

Since these devices were too thin for MIP signal detection, the radiation detection capabilities of these diodes using X-rays was investigated. Figure 9a,b show the dose linearity of the response of devices with different thicknesses of the substrate and two different areas of the junction. The sensors were irradiated by a 6 MV medical linear accelerator in standard conditions (source-to-surface distance of 100 cm, field size of 10×10 cm^2, and an equivalent water depth in a plastic phantom of 1.5 cm). Despite the sensors being configured in photovoltaic mode and the high degree of disorder of the substrate material, the adopted configuration of a doped area above an intrinsic amorphous layer allowed for the collection of the charge in proportion to the substrate thickness and the area of the sensor as expected.

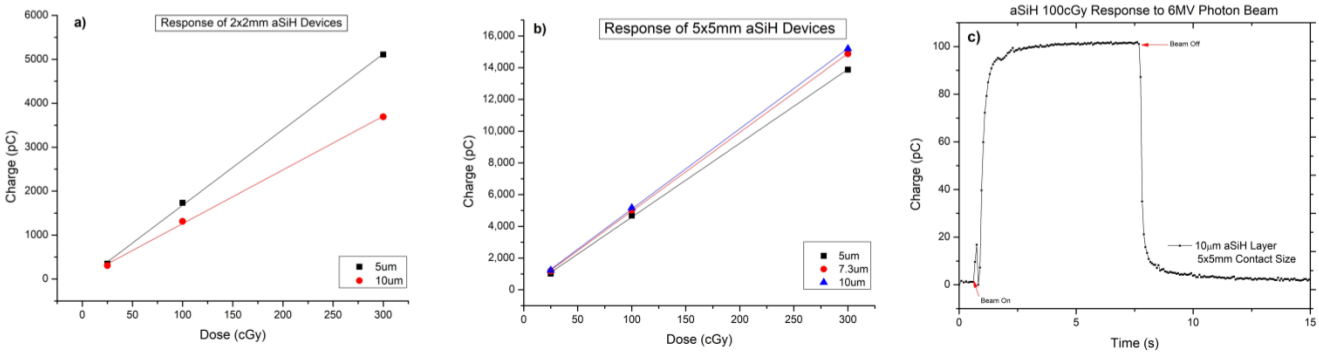

Figure 9. (**a**) Response of pad sensors with different thicknesses to 6 MV photon irradiation; (**a**) area of the sensor 2×2 mm^2; (**b**) area of the sensor 5×5 mm^2; (**c**) timing response of a 5×5 mm^2 10 μm-thick sensor.

In Addition, the timing response of the sample with 10 μm-thick substrate and an area of 5×5 mm^2 (Figure 9c) showed a stable response during the irradiation (beam-ON) within 2.2%, well within the expected fluctuations of the machine output [22].

Additional measurements were taken in order to determine the stabilization time after turn-on and the linearity of x-ray flux measurements. Figure 10 presents the measurements of the dark current versus time in a vertical diode under 25 V bias possessing a 10 μm active layer thickness and a 2×2 mm^2 active area. Figure 10a shows the measurement on a 2700 s time scale after turn-on and Figure 10b shows the same data on a 200 s time scale. These results shows that the measurement of the dark current became stable after about 200–250 s, with current fluctuations observed after this time remaining in the order of 80 pA.

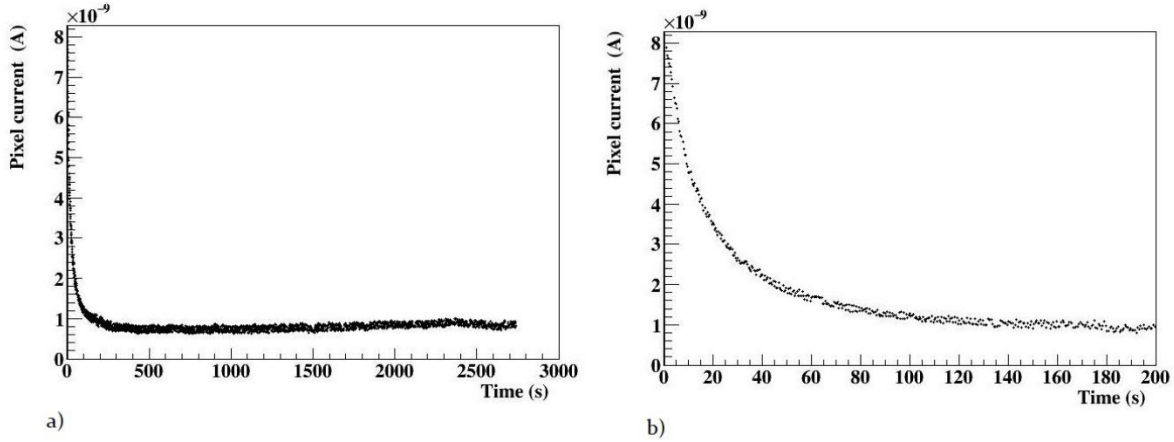

Figure 10. (**a**) Leakage current versus time in a 2700 s time scale, (**b**) leakage current versus time in a 200 s time scale.

Using the same device, we measured the linearity of response to X-rays using an X-ray tube with a tungsten cathode biased at 10 kV. Figure 11 shows the diode current response (after dark current subtraction) to irradiation versus the tube current for diode bias at 25 V (Figure 11a), 50 V (Figure 11b), and 100 V (Figure 11c). The resulting diode responses at all three applied biases displayed a good linearity of induced diode currents for X-ray tube currents in the range of 0 to 200 µA, with excellent linearities observed for tube currents above 30 µA.

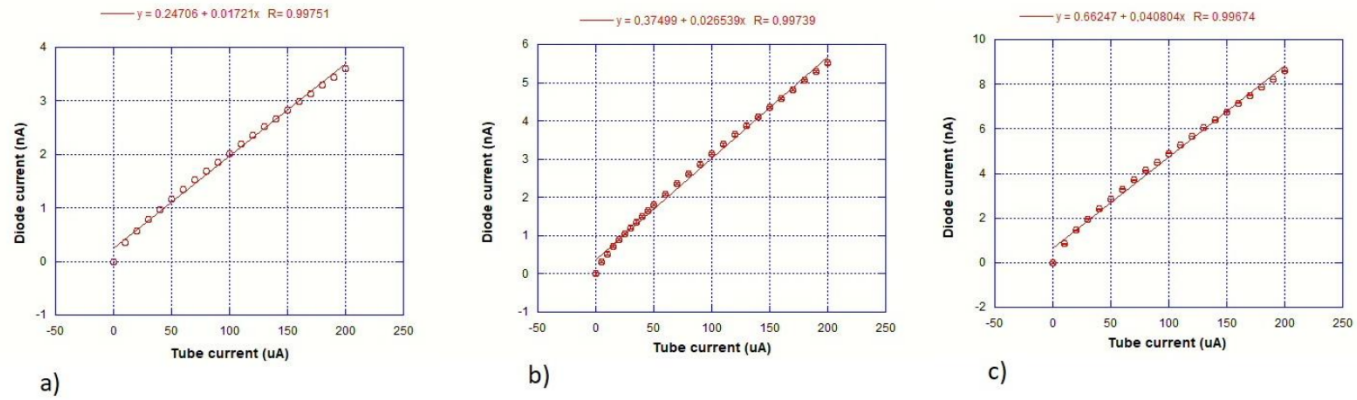

Figure 11. (**a**) Diode current versus X-ray tube current with diode biased at 25 V, (**b**) diode current versus X-ray tube current with diode biased at 50 V, (**c**) diode current versus X-ray tube current with diode biased at 100 V. The measurement were taken using a Keithley 2410C.

5. TCAD Simulation of a Full 3D Detector

Different geometrical configurations are being studied by means of device-level simulator Synopsys Sentaurus TCAD [23]. A proper description of the a-Si:H material has been included in the material library of Sentaurus TCAD [24]. In this study, full column electrodes, hybrid trench/column electrodes (mini trenches) and full trench electrodes were considered (Figure 12). For sake of computational effort, a 3D slice of the whole device depth was considered, looking at the electric field map distributions (steady-state simulations) and at the current vs. time response to a particle hit (transient simulation) of the different configurations.

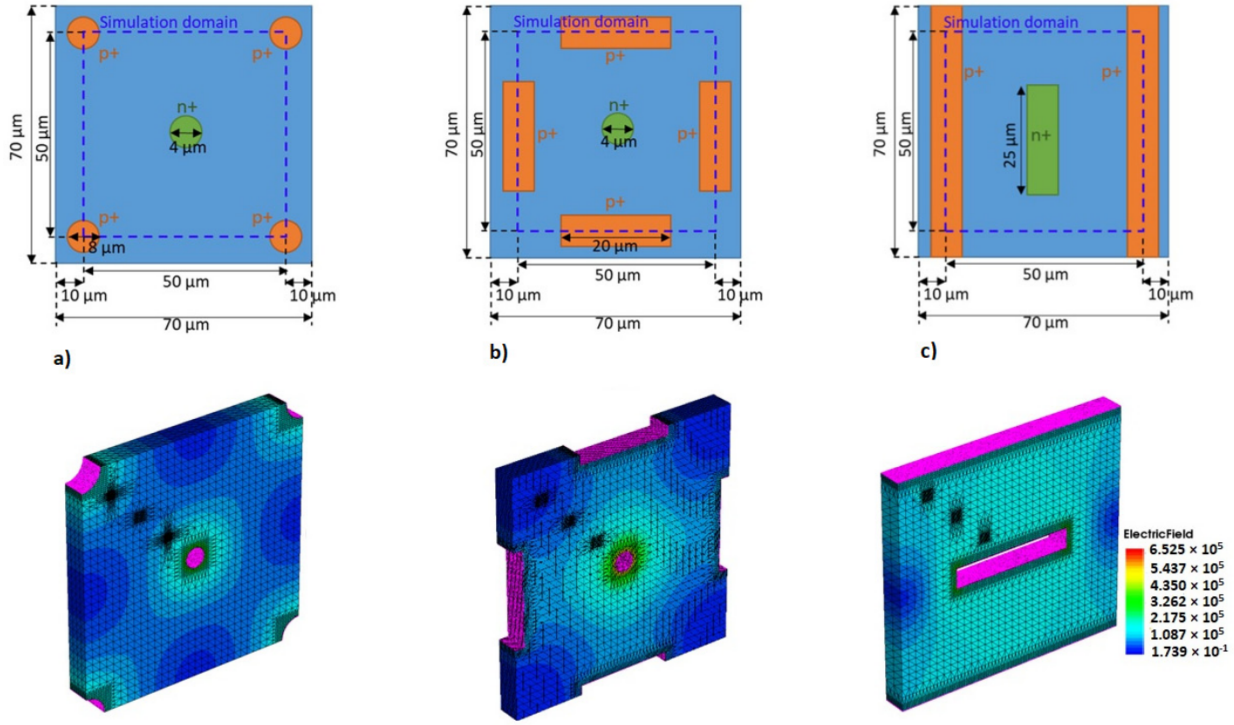

Figure 12. Simulated cells for the different 3D electrode configurations, from left to right: (**a**) full columns, (**b**) hybrid trenches/columns, (**c**) full trenches. The units for the electric field are V/cm.

Depending on the electric field distribution at the particle hit position, different amplitude and timing characteristics of the current response of the device can be appreciated. A faster and higher-current response can be seen with trench configurations (full lines in Figure 13) with respect to full column configurations (small dashed lines in Figure 13), in particular for particle hits close to the read-out electrode (blue and green curves in Figure 13). All currents in the graph were calculated for a 300 V bias.

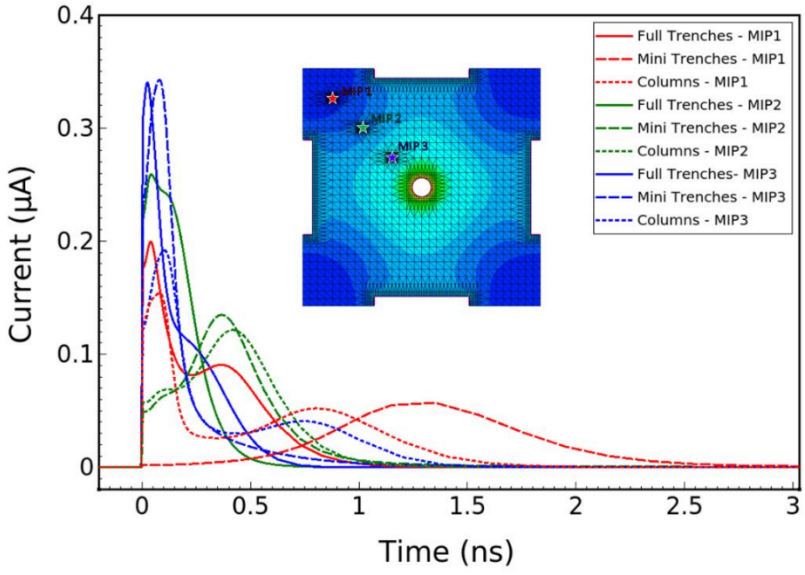

Figure 13. TCAD simulation results of the current pulse generated by an incident MIP. Current pulses are shown for MIPs incident on 3D architectures possessing full-trench (solid lines), mini-trench (large dashes), and full-column (small dashes) electrode configurations. Results are presented for MIPs incident in three various positions: MIP1 (red), MIP2 (green), and MIP3 (blue).

By integrating the time responses at the read-out electrode, the charge collection properties of the different configurations at different biasing conditions can be evaluated. This study enabled the choice of the optimal detector configuration.

6. Conclusions and Outlook

The fabrication of a 3D a-Si:H particle detector as described in this paper presents a new detector technology based on the peculiar properties of this material. A preliminary description of this fabrication process has already been given in another paper [25]. The fabrication process has been described here in detail and the R&D process towards the clarification of the feasibility of the detectors has been explained. The early results of the first generation of prototypes have been presented, demonstrating the capability of producing a working planar p-i-n diode with a quite low leakage current. We consider the first phase of prototype development to be satisfactory and have begun the second phase.

Detectors will be also tested after fabrication with radioactive sources like ^{90}Sr, electron accelerators, and collimated X-ray sources. After this, preliminary test detectors will be irradiated with protons, neutrons, and gamma rays from a cobalt-60 source for the evaluation of displacement and ionization damage. A new test run with the above-mentioned sources is foreseen.

In order to obtain charge collection efficiency maps of charge particles interacting with the detector, a test at the Australian Nuclear and Science Technology Organization (ANSTO—Lucas Heights—NSW, Australia) Ion Beam Induced Charge facility (IBIC) is also foreseen. The IBIC technique will be used to measure the charge-collection efficiency of the 3D device under test (DUT) using a ~1 μm spot size-focused ion beam scanning the DUT surface. The response of the DUT stimulated by the particle is correlated with the position of the beam, allowing a map of the efficiency of the device to be created [26,27]. The IBIC measurements will be performed using the heavy ion microprobe upon the ANTARES 10 MeV Tandem Accelerator. Various sources are available, including the 5.5 MeV helium ion beam with a range of 28 μm in silicon, which has already been used successfully in previous works [28].

The device will be also evaluated as a dosimeter using X-ray beams for imaging (keV energy range) and therapeutic applications (MeV energy range). The presence of two doping species allows for the use of these devices in photovoltaic mode (with no bias applied across the contacts). This property is particularly important for dosimetry, where a continuous current is read out from the device and dark currents limit the minimum threshold of the detectable dose delivered. The prototype test structures fabricated within the 3D-SiAm collaboration have demonstrated exceptionally low leakage currents and stable, linear responses to delivered doses via X-ray irradiations. These promising results verify the quality of the substrate, and the employed implantation methods are sufficient to guarantee the required MV X-ray response sensitivity and reproducibility outlined in the Code of Practice for dosimetric measurements [29].

The wide range of materials onto which a-Si:H can be deposited on opens up the possibility of the direct deposition of the detector material onto the readout chip. This feature has already been exploited in the past [2]. This detector technology, called TFA (thin film on ASIC), gave the best results in terms of signal-to-noise ratio in a planar a-Si:H detector for MIP detection (S/N ratio of 5 for an MIP). The deposition of a planar detector on the present technology front-end chip may increase this signal-to-noise ratio to higher values. Furthermore, a new technological frontier for the future may be the direct deposition of a 3D a-Si:H detector on the readout chip. The usage of DRIE technology for the fabrication of electrodes with two different lengths and selective implantation on different finger-type electrodes will allow for the fabrication of a detector like the one shown in Figure 14, where the n-type electrode reaches the readout pad of the readout chip and the p-type electrode does not reach the readout chip. After ion implantation, a passivation and a metallization layer to distribute the biasing contacts to the p-type electrodes will be added.

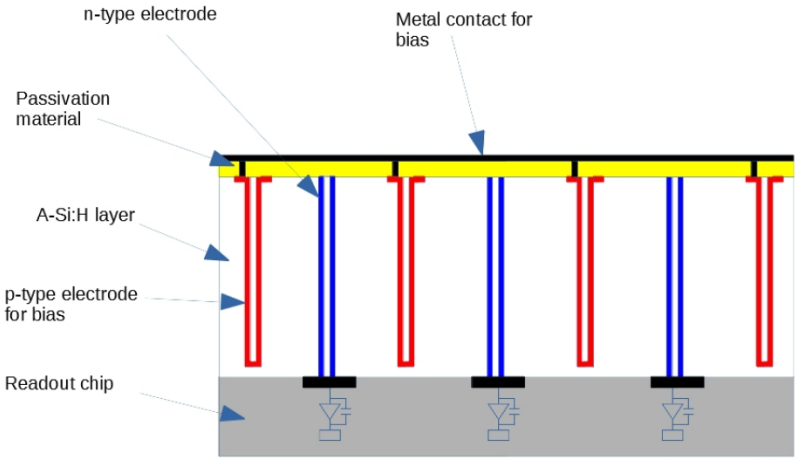

Figure 14. 3D a-Si:H detector deposited on a readout chip. N-type electrodes are connected directly on the readout pad of the chip, whereas p-type electrodes are connected to a common biasing plane.

7. Patents

The a-Si:H 3D detector is patented in Italy (patent number 102018000010735) and is patent pending in Europe (application number EP19831899.0) and in the U.S. (application number 17297441).

Author Contributions: Conceptualization, coordination, and editing, M.M.; nanofabrication, N.W., S.D., M.B. (Maurizio Boscardin), M.C. (Michele Crivellari), G.V., A.P.C., G.M., A.G.M. and S.R.; I/V testing, F.M., A.R., L.F. and O.H.A.; X-ray testing and dosimetry L.S., K.K., M.P., M.L., G.A.P.C., G.C., I.C. and C.T.; test setups, M.B. (Marco Bizzarri), M.C. (Mirco Caprai), M.I. and A.P.; simulations, D.P., A.S., A.M., M.P. and M.L. All authors have read and agreed to the published version of the manuscript.

Funding: The research was funded by INFN Scientific Committee 5 under the experiment name 3D-SiAm and by INFN Committee for Technology Transfer under the experiment name INTEF-3D-SiAm. Additional funds came from Fondazione Cassa di Risparmio di Perugia (RISAI project n. 2019.0245).

Data Availability Statement: The data presented in this study are available in article.

Conflicts of Interest: The authors declare no conflict of interest.

References

1. Wyrsch, N.; Ballif, C. Review of amorphous silicon based particle detectors: The quest for single particle detection. *Semicond. Sci. Technol.* **2016**, *31*, 103005. [CrossRef]
2. Despeisse, M.; Anelli, G.; Jarron, P.; Kaplon, J.; Moraes, D.; Nardulli, A.; Powolny, F.; Wyrsch, N. Hydrogenated amorphous silicon sensor deposited on integrated circuit for radiation detection. *IEEE Trans. Nucl. Sci.* **2008**, *55*, 802–811. [CrossRef]
3. Rech, B.; Wieder, S.; Siebke, F.; Beneking, C.; Wagner, H. Material basis of highly stable a-Si:H solar cells. *Mater. Res. Soc. Symp. Proc.* **1966**, *420*, 33. [CrossRef]
4. Shah, S.; Dutta, J.; Wyrsch, N.; Prasad, K.; Curtins, H.; Finger, F.; Howling, A.; Hollenstein, C. VHF plasma deposition: A comparative study. *Mater. Res. Soc. Proc.* **1992**, *258*, 15–26. [CrossRef]
5. Paquin, L.; Masson, D.; Wertheimer, M.R.; Moisan, M. Amorphous silicon for photovoltaics produced by new microwave plasma-deposition techniques. *Can. J. Phys.* **1985**, *63*, 831–837. [CrossRef]
6. Mahan, A. Hot wire chemical vapor deposition of Si containing materials for solar cells. *Sol. Energy Mater. Sol. Cells* **2003**, *718*, 299–327. [CrossRef]
7. Despeisse, M.; Anelli, G.; Commichau, S.; Dissertori, G.; Garrigos, A.; Jarron, P.; Miazza, C.; Moraes, D.; Shah, A.; Wyrsch, N.; et al. Characterization of 13 and 30 µm thick hydrogenated amorphous silicon diodes deposited over CMOS integrated circuits for particle detection application. *Nucl. Instrum. Methods A* **2004**, *518*, 357–361. [CrossRef]
8. Spear, W.E.; Lecomber, P.G. Electronic properties of substitutionally doped amorphous Si and Ge. *Philos. Mag.* **1976**, *33*, 935–949. [CrossRef]
9. Street, R.A. Doping and the fermi energy in amorphous silicon. *Phys. Rev. Lett.* **1982**, *49*, 1187–1190. [CrossRef]
10. Spear, W.E.; Lecomber, P.G. Electrical and photoconductive properties of ion implanted amorphous silicon. *J. Non-Cryst. Sol.* **1980**, *35–36*, 327–332.

11. Demond, F.J.; Muller, G.; Kalbizer, S.; Spear, W.E.; Lecomber, P.G. Hydrogen in gas phase and ion implantation doped amorphous silicon. *Nucl. Instrum. Methods A* **1981**, *191*, 59–62. [CrossRef]
12. Chikamura, T.; Aoki, Y.; Yano, K.; Komeda, T.; Ishihara, T. Spectral response of boron-implanted amorphous silicon Schottky diode. *J. Appl. Phys.* **1985**, *57*, 2280. [CrossRef]
13. Pochet, T.; Dubeau, J.; Equer, B.; Karar, A.; Hamel, L.A. High reverse voltage amorphous silicon p-i-n diodes. *J. Appl. Phys.* **1990**, *68*, 1340–1344. [CrossRef]
14. Fujieda, I.; Cho, G.; Drewery, J.; Jing, T.; Kaplan, S.N.; Perez-Mendez, V.; Qureshi, S.; Wildermuth, D.; Street, R.A. Field Profile Tailoring in a-Si:H Radiation Detectors. *Mater. Res. Soc. Symp. Proc.* **1990**, *192*, 399–404. [CrossRef]
15. Perez-Mendez, V.; Cho, G.; Drewery, J.; Jing, T.; Kaplan, S.N.; Qureshi, S.; Wildermuth, D.; Fujieda, I.; Street, R.A. Amorphous Silicon Based Radiation Detectors. *J. Non-Cryst. Sol.* **1991**, *137–138*, 1291–1296. [CrossRef]
16. Wyrsch, N.; Miazza, C.; Dunand, S.; Ballif, C.; Shah, A.; Despeisse, M.; Moraes, D.; Powolny, F.; Jarron, P. Radiation hardness of amorphous silicon particle sensors. *J. Non-Cryst. Solids* **2006**, *352*, 1797–1800. [CrossRef]
17. Fujieda, I.; Cho, G.; Conti, M.; Drewery, J.; Kaplan, S.N.; Perez-Mendez, V.; Qureshi, S.; Street, R.A. Improved charge collection of the buried p-i-n a-Si:H radiation detectors. *IEEE Trans. Nucl. Sci.* **1990**, *37*, 124–128. [CrossRef]
18. Dalla Betta, G.-F.; Boscardin, M.; Darbo, G.; Mendicino, R.; Meschini, M.; Messineo, A.; Ronchin, S.; Sultan, D.M.S.; Zorzi, N. Development of a new generation of 3D pixel sensors for HL-LHC. *Nucl. Instrum. Methods A* **2016**, *824*, 386–387. [CrossRef]
19. Forcolin, G.T.; Mendicino, R.; Boscardin, M.; Lai, A.; Loi, A.; Ronchin, S.; Vecchi, S.; Dalla Betta, G.-F. Development of 3D trenched-electrode pixel sensors with improved timing performance. *J. Instrum.* **2019**, *14*, C07011. [CrossRef]
20. Tsai, C.C.; Knights, J.C.; Chang, G.; Wacker, B. Film formation mechanisms in the plasma deposition of hydrogenated amorphous silicon. *J. Appl. Phys.* **1986**, *59*, 2996–3001. [CrossRef]
21. Hsu, C.M.; Battaglia, C.; Pahud, C.; Ruan, Z.; Haug, F.J.; Fan, S.; Ballif, C.; Cui, Y. High-Efficiency Amorphous Silicon Solar Cell on a Periodic Nanocone Back Reflector. *Adv. Energy Mater.* **2012**, *2*, 628–633. [CrossRef]
22. Ravichandran, R.; Binukumar, J.P.; Davis, C.A.; Krishnamurthy, K.; Sivakumar, S.S. Evaluation methods for detecting changes in beam output and energy in radiation beams from high-energy linear accelerators. *J. Med. Phys.* **2007**, *32*, 92–96. [CrossRef]
23. TCAD—Technology Computer Aided Design (TCAD) | Synopsys. Available online: https://www.synopsys.com/silicon/tcad.html (accessed on 27 September 2021).
24. Davis, J.A.; Boscardin, M.; Crivellari, M.; Fanò, L.; Large, M.; Menichelli, M.; Morozzi, A.; Moscatelli, F.; Movileanu-Ionica, M.; Passeri, D.; et al. Modeling a Thick Hydrogenated Amorphous Silicon Substrate for Ionizing Radiation Detectors. *Front. Phys.* **2020**, *8*, 158. [CrossRef]
25. Menichelli, M.; Boscardin, M.; Crivellari, M.; Davis, J.; Dunand, S.; Fanò, L.; Moscatelli, F.; Movileanu-Ionica, M.; Petasecca, M.; Piccini, M.; et al. 3D Detectors on Hydrogenated Amorphous Silicon for particle tracking in high radiation environment. *J. Phys. Conf. Ser.* **2020**, *1561*, 012016. [CrossRef]
26. Siegele, R.; Cohen, D.D.; Dytlewski, N. The ANSTO high energy heavy ion microprobe. *Nucl. Instrum. Methods B* **1999**, *158*, 31–38. [CrossRef]
27. Ziegler, J.F.; Ziegler, M.D.; Biersack, J.P. SRIM—The stopping and range of ions in matter. *Nucl. Instrum. Methods B* **2010**, *268*, 1818–1823. [CrossRef]
28. Alhujaili, S.F.; Davis, J.A.; Davies, J.; Lerch, M.L.; Rosenfeld, A.B.; Petasecca, M. Characterization of an "Edgeless" Dosimeter for Angular Independent Measurements in Advanced Radiotherapy Treatments. *IEEE Trans. Radiat. Plasma Med. Sci.* **2019**, *3*, 579–587. [CrossRef]
29. *IAEA TRS483*; International Atomic Energy Agency (IAEA): Vienna, Austria, 2017.